Formation of Small Bubbles in an Electric Field

K. J. Ptasinski[a]; F. L. S. Geurts[a]; A. J. P. M. Staring[a]; E. J. M. Van Heesch[b]; P. J. A. M. Kerkhof[c]
[a] DEPARTMENT OF CHEMICAL ENGINEERING, UNIVERSITY OF TECHNOLOGY, MB EINDHOVEN, THE NETHERLANDS [b] DEPARTMENT OF ELECTRICAL ENGINEERING, UNIVERSITY OF TECHNOLOGY, MB EINDHOVEN, THE NETHERLANDS [c] DEPARTMENT OF CHEMICAL ENGINEERING, EINDHOVEN UNIVERSITY OF TECHNOLOGY, MB EINDHOVEN, THE NETHERLANDS

PLEASE SCROLL DOWN FOR ARTICLE

Formation of Small Bubbles in an Electric Field

K. J. PTASINSKI, F. L. S. GEURTS, and A. J. P. M. STARING
DEPARTMENT OF CHEMICAL ENGINEERING

E. J. M. VAN HEESCH
DEPARTMENT OF ELECTRICAL ENGINEERING

P. J. A. M. KERKHOF
DEPARTMENT OF CHEMICAL ENGINEERING

EINDHOVEN UNIVERSITY OF TECHNOLOGY
P.O. BOX 513, 5600 MB EINDHOVEN, THE NETHERLANDS

ABSTRACT

The formation of gas bubbles injected into an insulating liquid was studied under the influence of a nonuniform electric field. The electrode configuration used consisted of a charged capillary opposite a grounded ring, and gas bubbles were formed at the capillary tip. The experimental part of the investigation afforded insight into the mechanism of bubble formation, which is influenced by the existence of corona discharge. Based on the balance of forces at bubble detachment, a theoretical model was developed to predict the variation in bubble sizes. The theory agrees closely with experimental results over a range of applied voltages where the corona discharges were absent.

INTRODUCTION

Efficient separation processes usually rely on energy input in the form of thermal or mechanical energy and on external forces such as gravity, pressure, or centrifugal forces. The application of electric fields to enhance separations has been practiced for a long time but it is still one of the promising techniques. A number of reviews summarize the work that has been done on the subject to date (1, 2). The use of an ac or dc electric

field in separation technology has been demonstrated to improve conventional processes, e.g., liquid–liquid coalescence (3), filtration (4), or solvent extraction (5), as well as to develop new separation processes, e.g., electrical field-flow fractionation (6).

Gas absorption in liquid is one of the basic separation techniques employed in many components of chemical industrial processes, such as gas separation for product recovery or gas purification, catalytic slurry reactors, bioreactions, coal liquefaction, etc. Gas–liquid absorption, like many other mass transfer processes, involves direct contact between a dispersed gas phase in the form of bubbles and a continuous liquid phase. The mass transfer rate of such systems is proportional to the interfacial surface area and the overall mass transfer coefficient. One way to increase the transfer rate is by increasing the interfacial area between the phases, which means a size reduction of the gas bubbles.

The common method of gas dispersion in a liquid applies gas by forcing it through orifices, perforated plates, or other porous sparging devices submerged in a liquid, as in bubble and plate columns. In practice, more intensive dispersion can be created by an extra input of mechanical energy into the liquid, as in mechanically agitated and rotated devices, or by using impinging jets. Although such devices achieve some bubble size reduction, they represent inefficient use of energy because most of the energy supplied is expended for liquid agitation and not for an increase of the interfacial area. Other major disadvantages of traditional gas–liquid contactors are a rather large size of equipment, comparatively high power requirement, and a limited control of gas residence time.

Electrical gas–liquid contactors, in which the interfacial area is increased by an electric field produced by an external energy source, are very promising in this respect. The possibility of size reduction of gas bubbles being generated from the tip of a single needle was first reported in 1977 by Zaky and Nosseir (7). They found that under a strong nonuniform electric field, the size of air bubbles injected into insulating liquids decreased with increasing dc voltage. Sato et al. (8), using a similar method, demonstrated the cloudy-bubble generator that made it possible to produce extremely small nitrogen bubbles in water. A crowd of cloudy bubbles with a mean diameter of 85 μm was obtained when the average electric field strength was about 100 kV/m. Gas–liquid dispersions in insulating liquids formed under nonuniform dc fields were studied experimentally (9) and subsequently theoretically (10) by Ogata et al. They also reported beneficial field effects on the bubble size reduction, and, moreover, some physical processes participating in the bubble dispersion mechanism were discussed (10). The analysis of process efficiency presented in their study reveals that the energy needed for bubble size reduction in nonpolar liq-

uids is some orders of magnitude lower than that of stirred vessels. On the other hand, the energy needed for bubble dispersion in polar liquids can be of the same order of magnitude as that needed for mechanically agitated devices.

Recently, van Heesch et al. (11) developed an improved electrical technique for bubble disruption in highly conducting liquids. This new method applies high frequency pulsed electric fields in the range of corona discharges. With this method it is possible to generate extremely small air bubbles with a mean size of 50 μm in tap water at a power input of a few watts.

It should be noted that electrical dispersion techniques that can produce very small bubbles may have wider applications in laboratory and industry, such as foam fractionation, flotation, including separation using "microgas dispersions" in the form of colloidal gas aphrons (12).

In spite of the advantages of the electrical dispersion method in various application fields, there is very little information in the open literature concerning the mechanism of bubble formation. This paper describes part of an ongoing study to investigate the size of bubbles formed under a strong nonuniform electric field. In the work described here, gas bubbles were generated from the tip of a charged single capillary placed opposite of a grounded ring electrode. The purpose of this paper is to develop a mathematical analysis of the bubble formation in an electric field, and to compare the predictions of the model concerning the size of bubbles with the results of the experimental investigations.

EXPERIMENTAL

A schematic diagram of the experimental apparatus is shown in Fig. 1. It consists essentially of a rectangular cell with a capillary that forms a bubbling system, and a high voltage generator connected to the capillary. The cell, Fig. 2, was made of glass and its dimensions were 4 × 4 × 14 cm. Bubbles were formed at the tip of the stainless steel capillary mounted at the bottom of the cell. The capillary had an inner diameter of 0.30 mm and an outer diameter of 0.60 mm. The capillary tip was located 1 mm above the PTFE plate, which surrounded the capillary in order to reduce the leakage current. The grounded ring electrode was situated 1 cm above the capillary tip, and the diameter of the grounded ring was 2.1 cm. The nonuniform electric field was produced by applying a negative dc potential to the capillary. A dc field was applied using a Wallis power supply with a variable voltage of 0 to 15 kV and a maximum current of 30 mA.
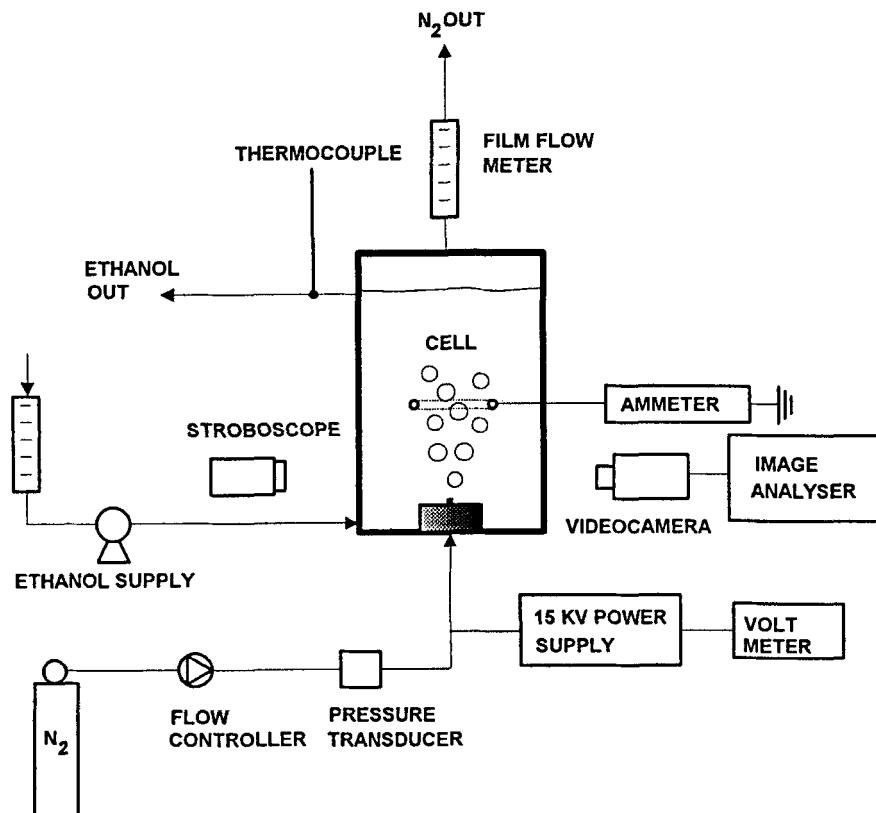
FIG. 1   Experimental apparatus used in bubble formation studies.

Experiments were carried out with nitrogen gas, while ethanol was used as the liquid phase. The system properties are summarized in Table 1. Nitrogen was supplied from a cylinder through a Brooks model 5850TR mass flow controller, and the flow rate of gas leaving the cell was additionally measured by a film flowmeter. The nitrogen pressure in the capillary was measured with a Hottinger Baldwin pressure transducer in order to evaluate an additional electric pressure caused by the electric field. Ethanol was passed from a tank through a thermostat into the cell, so that the liquid temperature in the cell was kept constant.

The bubble formation process was examined with a stroboscopic light (Philips) at a frequency of 25 Hz, along with a video/image analysis sys-
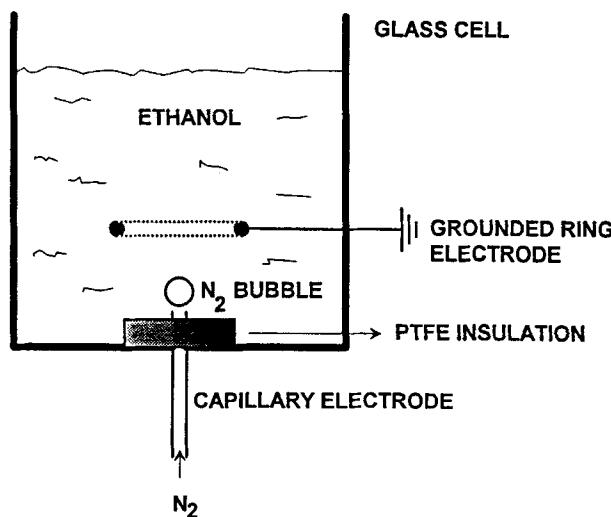
FIG. 2   Simplified schematic of bubble formation system.

tem. This system consisted of several components: a video camera (HTH MS, Holland), a monitor (Philips), and software for image analysis (TIM Image Analyser, DIFA, Holland). In this work, equivalent diameters of individual bubbles were calculated by the image analyzer by matching the projected area of each bubble to that of a sphere of the same diameter. For each run, two hundred bubbles were measured with the image analyzer to determine the average bubble size.

TABLE 1
Physical Properties of Fluids Used

Property at 20°C	Nitrogen	Ethanol
Density (kg/m^3)	1.130	785
Viscosity (Pa·s)	1.76×10^{-5}	1.04×10^{-3}
Interfacial tension (N/m)	→	23.1×10^{-3}
Dielectric constant	1.0	24.3
Electrical conductivity (S/m)	—	6.4×10^{-6}

EFFECT OF AN ELECTRIC FIELD IN BUBBLE FORMATION

The behavior of gas bubbles generated under an electric field has previously been described by Sato (13), and later by Ogata (9, 10), and will not be repeated here. However, some basic phenomena taking place during bubble formation will be restated as they will form the foundation for a theoretical model presented in the next section.

Typical images of bubbles obtained with the previously mentioned technique are shown in Fig. 3 for various applied voltages. The pictures clearly illustrate the beneficial effect of the electric field on bubble size reduction.
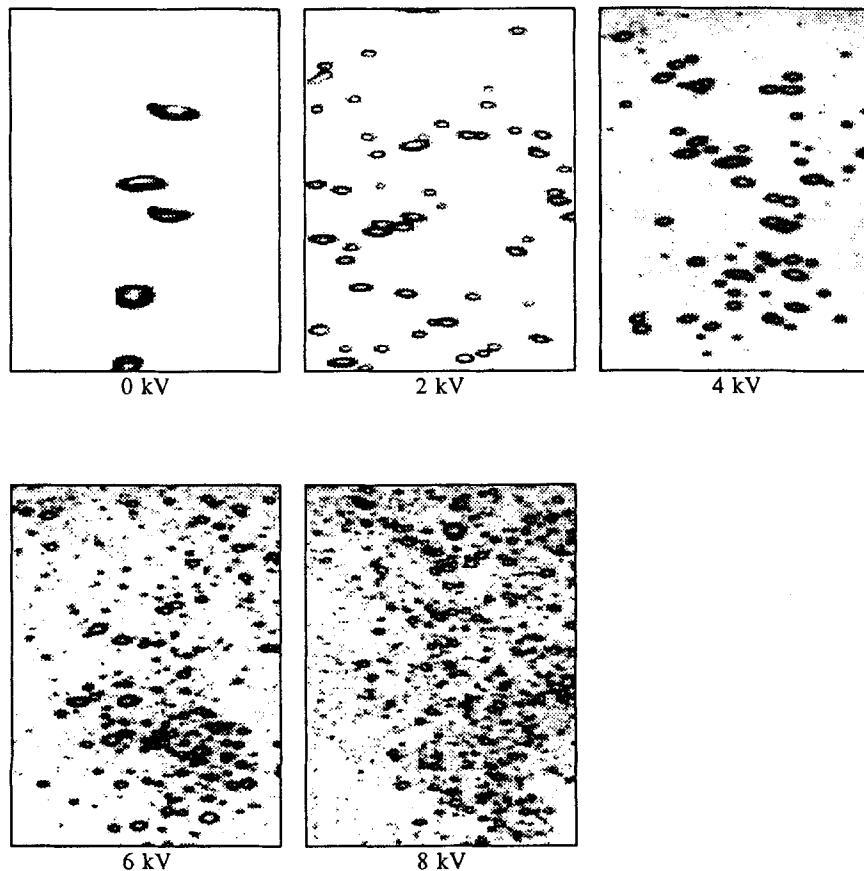
FIG. 3   Typical images of bubbles for various voltages. Gas flow rate $Q = 0.5$ cm^3/s.

The average diameter of the bubbles shown in Fig. 3 ranges from 2.7 mm under zero field to 0.25 mm at the highest applied voltage (8 kV).

In the course of the experiments, two distinct regimes of bubble formation could be observed, depending upon the applied voltage, and, more specifically, on the occurrence of corona discharges. At low capillary potentials, bubbles were produced sequentially and their sizes were distributed in a relatively narrow range. At higher potentials, in the present case above the value of 3.5 kV, the existence of corona discharge at the capillary tip was observed, and discrete bubbles were no longer formed. Instead, the capillary sprayed much smaller bubbles, which moreover gave rise to a much wider distribution of bubble sizes.

The two distinct regimes of bubble formation can also be deduced from Fig. 4, which shows how the electric pressure at the capillary tip and the conduction current between the electrodes vary with the applied voltage. Electric pressure was calculated as the difference between the gas pressure measured at the inlet to the capillary at the given applied voltage and at zero field. It is evident from Fig. 4 that the graphs of electric pressure and conduction current are divided into two regions and the transition takes place at an applied voltage of 3.5 kV. The electric pressure increases
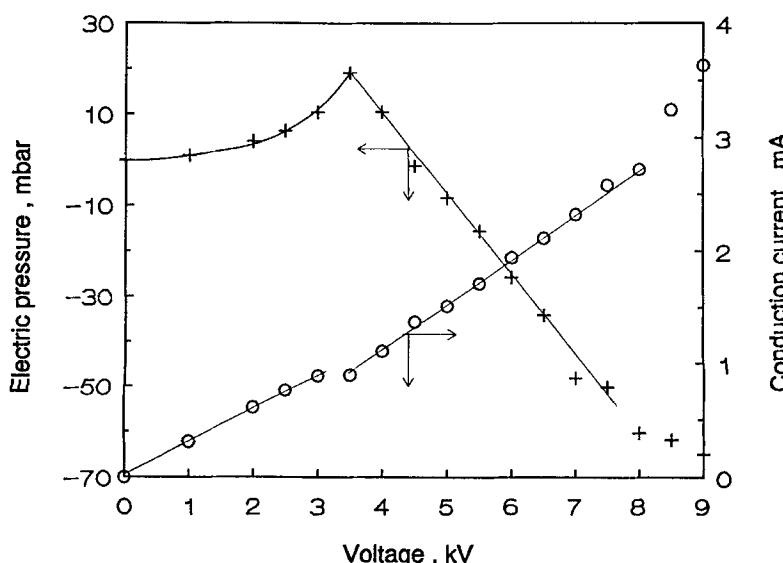

FIG. 4   Effect of the applied voltage on electric pressure and conduction current at a gas flow rate of 0.5 cm³/s.

in the first region with the applied voltage up to a maximum near the mentioned value of 3.5 kV, and in the second region it is lowered as soon as the corona discharge occurs. On the other hand, the conduction current which is due to leakage increases in the second region more steeply with the applied voltage, compared to that observed at lower voltage.

All the above-mentioned phenomena suggest different mechanisms of bubble formation depending on the range of applied voltage. In the present paper the theory of bubble formation has been developed for the first range of bubble formation, that is, when the corona discharges are absent.

THEORETICAL MODEL

At present, a general theory which explains the formation of gas bubbles in nonuniform electric field is not available, though Ogata (10) discussed some phenomena contributing to the mechanism of bubble formation at the nozzle. The most important of these phenomena are bubble elongation due to the applied electric field, electrostatic pressure due to polarization effects in dielectrics, and hydrodynamic flow generated by the electric field. On the other hand, Garton and Krasucki (14) presented a theoretical treatment of electrical forces acting on a bubble immersed in an insulating liquid and subjected to a uniform electric field between parallel plate electrodes.

The following theoretical analysis of the process of bubble formation in a nonuniform electric field is developed to describe the way in which gas bubbles are formed at the capillary tip in the range of applied voltages where corona discharges are absent. The theoretical model presented in this paper follows that developed by Mersmann (15) for bubble formation in the absence of an electric field. According to the general classification of bubble formation models presented by Tsuge (16), the model by Mersmann falls within the range of experimental conditions (at zero field) applied in this work. In this model the bubble size at the moment of detachment is calculated from the equilibrium of forces during bubble formation. In the overall force balance equation, forces due to surface tension, drag, and bouyancy (gravity) are considered:

$$F_s + F_d = F_b \tag{1}$$

The interfacial tension force, F_s, does not depend on the bubble size and is given by

$$F_s = \pi d\sigma \tag{2}$$

where d is the capillary inner diameter and σ is the interfacial tension.

The force on the bubble due to drag, F_d, was expressed by Mersmann as

$$F_d = \frac{\pi K Q^2 \rho_1 d}{\sigma d_B^3} \tag{3}$$

where d_B is the bubble diameter, Q is the gas flow rate, and ρ_1 is the liquid density. The constant K, which includes the drag coefficient, has an average value of 15 on the basis of the experimental data analyzed by Mersmann. The bouyancy force, F_b, which also depends on the bubble diameter, is

$$F_b = \frac{\pi}{6} d_B^3 (\rho_1 - \rho_2) g \tag{4}$$

where ρ_2 is the gas density and g is the acceleration constant due to gravity.

The bubble size follows from Eqs. (1)–(4), neglecting the gas density in Eq. (4):

$$d_B = \left[\frac{3d\sigma}{\rho_1 g} + \sqrt{\left(\frac{3d\sigma}{\rho_1 g} \right)^2 + \frac{15 Q^2 d}{g}} \right]^{1/3} \tag{5}$$

In analyzing the influence of an electric force on bubble formation, the reduction in bubble size can be anticipated, provided this force is applied in the same direction as the bouyancy force and opposing surface and drag forces, so the balance of forces becomes

$$F_s + F_d = F_b + F_e \tag{6}$$

The terms F_s, F_d, and F_b correspond to those given in Eqs. (2)–(4), while the electric force F_e cannot be calculated straightforwardly. Nevertheless, Eq. (6) can be used to calculate the bubble size at detachment in the presence of an electric field, provided the electric force is known. From Eqs. (2)–(4) and (6), the following expression analogous to Eq. (5) is then obtained:

$$d_B = \left[\frac{3d\sigma}{\rho_1 g} - \frac{3F_e}{\pi \rho_1 g} + \sqrt{\left(\frac{3d\sigma}{\rho_1 g} \right)^2 - \frac{18 d\sigma F_e}{\pi \rho_1^2 g^2} + \left(\frac{3F_e}{\pi \rho_1 g} \right)^2 + \frac{15 Q^2 d}{g}} \right]^{1/3} \tag{7}$$

The balance of forces, Eq. (6), can be rewritten by substituting Eqs. (2)–(4) in order to calculate the net electric force which is needed to detach bubbles of the specified size d_B:

$$F_e = \pi d\sigma + \frac{15 \pi Q^2 \rho_1 d}{\sigma d_B^3} - \frac{\pi \rho_1 g d_B^3}{\sigma} \tag{8}$$

Table 2 gives values of F_s, F_d, and F_b calculated from Eqs. (2)–(4), respectively, and values of F_e calculated from Eq. (8) as a function of the bubble diameter d_B. The results of force calculations show that under zero field conditions the forces F_s, F_d, and F_b are of the same order of magnitude, which supports the choice of the model of Mersmann. On the other hand, the results presented indicate that significantly large electric forces are needed to form bubbles of small sizes.

The primary question of this investigation concerns the nature of an electric force F_e which contributes to a bubble detachment, and its evaluation from the known values of electric field strength, electrode configuration, and system properties. As was reviewed by Ptasinski (1), the total electric force on a dielectric involves the Coulomb force, the polarization force, and the force due to electrostriction. The assumption made in the development of this model is that the polarization forces are predominant, whereas contributions of other electric forces are likely to be negligible. The Coulomb force due to free charges seems to be rather small in an insulating liquid in the absence of corona discharges. The electrostrictive terms do not contribute to the net electric force acting on a gas bubble in a liquid, as shown by Garton and Krasucki (14).

The forces due to polarization exerted on an uncharged gas bubble in an insulating dielectric liquid have been given by a number of investigators (14, 17). In order to describe these forces, the electric field has to be decomposed into a normal and a tangential component in respect to the bubble surface. The local electric stress, that is, the electric force per unit area acting on the gas–liquid boundary due to the tangential component of the field, is given by

$$P_{e,t} = \frac{1}{2}(\epsilon_1 - \epsilon_2)E_{2,t}^2 \tag{9}$$

where ϵ_1 and ϵ_2 are the permittivities of the liquid and the gas phase,

TABLE 2
Forces on Nitrogen Bubbles in Ethanol at the Detachment: $d = 0.3$ mm, $Q = 0.5$ cm³/s

Bubble diameter, d_B (mm)	Interfacial tension force, $F_s \times 10^4$ (N)	Drag force, $F_d \times 10^4$ (N)	Bouyancy force, $F_b \times 10^4$ (N)	Electric force, $F_e \times 10^4$ (N)
2.40	0.218	0.337	0.554	0
2.00	0.218	0.578	0.323	0.473
1.50	0.218	1.370	0.136	1.452
1.00	0.218	4.624	0.040	4.801

respectively, and $E_{2,t}$ is the tangential component of the field in the gas phase.

Similarly, the local electric stress due to the normal component of the field is given by

$$P_{e,n} = \frac{1}{2}\frac{\epsilon_2}{\epsilon_1}(\epsilon_1 - \epsilon_2)E_{2,n}^2 \tag{10}$$

where $E_{2,n}$ is the normal component of the field in the gas phase. Both electric stresses have directions normal to the boundary and they are inwardly directed, since in this case the permittivity of the dispersed gas phase ϵ_2 is lower than that of the continuous liquid phase ϵ_1. Hence, the total local electric stress acting on any point of the gas–liquid boundary is given by

$$P_{e,x} = \frac{1}{2}(\epsilon_1 - \epsilon_2)\left(E_{2,t}^2 + \frac{\epsilon_2}{\epsilon_1}E_{2,n}^2\right) \tag{11}$$

Note that $E_{2,t}$ and $E_{2,n}$ are the local components of the field, and they depend not only on the applied voltage and electrode spacing but also on the position on the bubble surface. This is not straightforward because the interaction of a nonuniform electric field with the two different fluid dielectrics in the neighborhood of the capillary tip can change the direction of the field lines at the curved gas–liquid interface. This fact makes the theoretical analysis of the nonuniform field difficult, and expressions for the total electric stresses acting on the bubble boundary, if derived by taking into account only the nominal or mean value of the field (10), are very rough. In the present paper the local electric stress $P_{e,x}$ was evaluated from Eq. (11) and from the local values of $E_{2,t}$ and $E_{2,n}$, which were computed numerically by the finite elements method with a two-dimensional field simulator (18).

Figure 5 shows an example of the computed variation of both field components as a function of the position on the bubble surface, measured along the perimeter line upward from the contact point between the bubble and the capillary tip. It is evident from this figure that the field strength is locally concentrated around the capillary tip. The field computations were carried out assuming a spherical gas bubble, as the elongation of bubbles by the electric field strength is negligible (14). In order to evaluate the electric force F_e contributed to a bubble detachment, the local electric stress $P_{e,x}$ has to be further decomposed into a vertical and a horizontal component. The net force, F_e, on the bubble boundary due to the electric field (see Eq. 6) is found by integrating the vertical component of electric stress over the surface of the bubble. This force acts upward because the
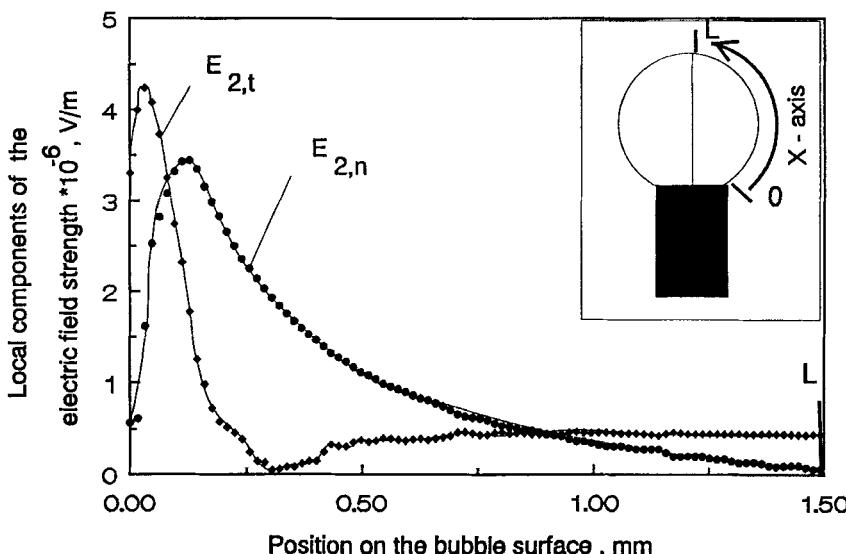
FIG. 5   Variations of tangential and normal components of the electric field strength as a function of the position on the bubble surface. Applied voltage $V = 2$ kV.

electric stress is inwardly directed and the field strength is higher at the lower part of the bubble. On the other hand, the results of integrating the horizontal component of electric stress will give the horizontally directed force, which might only give rise to bubble elongation.

The above-mentioned mechanism is similar to that operating during "dielectrophoresis." Dielectrophoresis in a nonuniform field does not require charged particles (drops, bubbles), while inert particles are attracted by polarization forces into regions of relatively lower electric field intensity when the permittivity of the dispersed phase is lower than that of the continuous one, that is, $\epsilon_2 < \epsilon_1$.

RESULTS AND DISCUSSION

Figure 6 shows a comparison between experimental diameters of bubbles formed in the electric field and bubble diameters predicted theoretically. The filled symbols represent the experimental values of the diameters as a function of the applied voltages. The solid line (open symbols) shows the bubble diameters computed with the theoretical model presented earlier together with the following procedure. For each value of the applied voltage, the total electric stress $P_{e,x}$ was calculated from Eq.
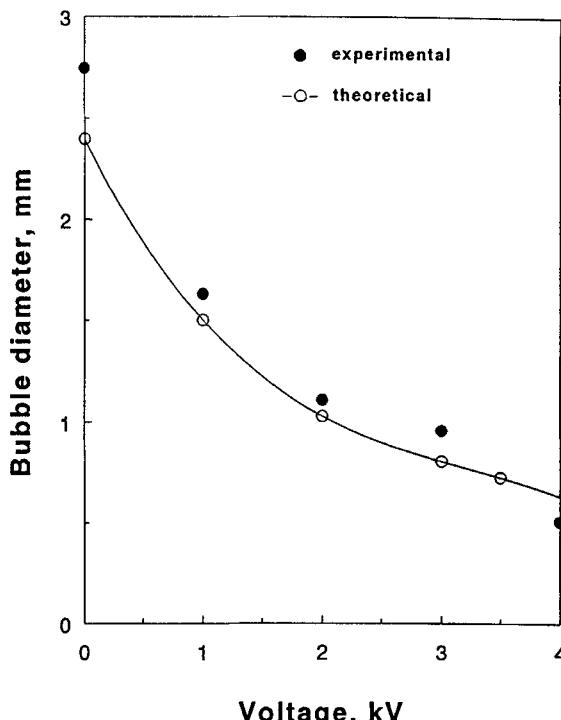
FIG. 6   Comparison between theoretical and experimental values of the bubble diameter
for various voltages. Gas flow rate $Q = 0.5$ cm³/s.

(11) with a two-dimensional field simulator for the electrode configuration
used in this work and for the experimental value of the bubble diameter
corresponding to the given value of the applied voltage. The results of
these calculations are shown in Fig. 7. A computer program was written
to evaluate the net upward electric force F_e according to the previously
presented procedure. Finally, the bubble diameter was calculated from
Eq. (7). The agreement between experimental bubble sizes and model
predictions shown in Fig. 6 is fairly good up to an applied voltage of 3.5
kV, that is, within the range where corona discharges are absent. More-
over, the results presented in Fig. 7 support the assumption of neglecting
bubble elongation because of the strongly asymmetric character of the
electric stress.

  Another representation of the model is provided in Fig. 8, where electric
forces calculated from the experiments are compared to those predicted
by the proposed model. The filled symbols in this figure represent electri-
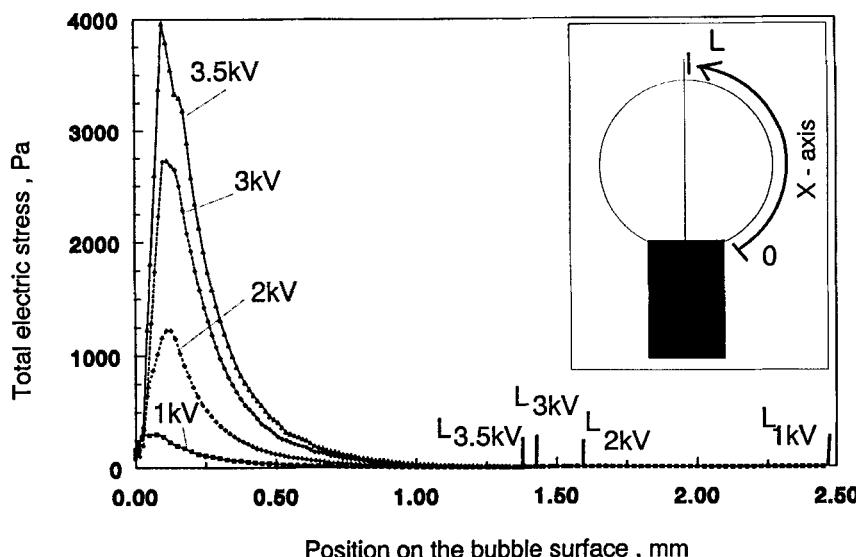
FIG. 7   Variations of total electric stress as a function of the position on the bubble surface
for various applied voltages.

cal forces calculated from Eq. (8) with the measured values of bubble
diameter. The solid line (open symbols) shows electrical forces which
were computed numerically for a given value of applied voltage, as de-
scribed above. It can be seen that the model curve follows the experimen-
tal points quite well at lower voltages, but the agreement in the 3.0 to 3.5
kV range is less satisfactory. At this range of applied potentials, the model
predicts higher electrical forces than needed, according to Eq. (8), to
detach the bubbles produced in the experiments.

Agreement between the theoretical and experimental forces at lower
voltages supports the assumption made in the model development con-
cerning the nature of the electric force as being due to the polarization
effects only. On the other hand, the agreement at higher voltages would
become better by assuming additional electric charges in the liquid phase.

The addition of bulk charge into a liquid lowers the local electric field
strength in the surrounding area of the bubble, and consequently the polar-
ization forces are reduced. In order to confirm this hypothesis, a two-
dimensional electric field simulator was used to calculate the required
bulk charge densities in a liquid which fit the experimental values of the
electric forces. Table 3 shows the obtained values of charge density calcu-
lated assuming a homogeneous charge distribution. Although a charge
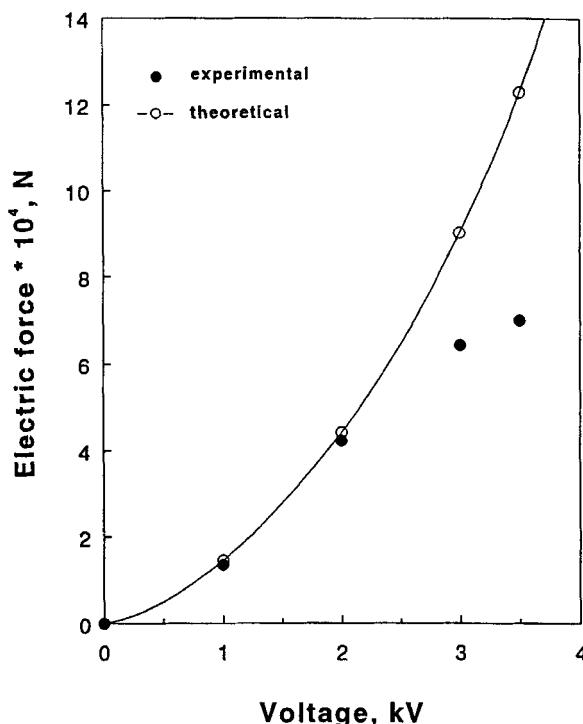
FIG. 8   Comparison between theoretical and experimental values of electric forces for various voltages. Gas flow rate $Q = 0.5$ cm³/s.

distribution is not likely to be homogeneous, it might give a good indication of the order of magnitude of the required charge. The maximal charge density in Table 3 is 40×10^{-5} C/m³, which corresponds to a concentration difference between positive and negative charges in the liquid equal to 4×10^{-9} mol/m³, assuming a single valency of both ions. On the other

TABLE 3
Bulk Charge Densities Calculated to Fit the Experimentally Found
Electric Forces

Applied voltage (kV)	Bulk charge density $\times 10^5$ (C/m³)
1	1
2	4
3	21
3.5	40

hand, the dissociation constant of ethanol is equal to 3×10^{-20} mol^2/L^2 (19), which corresponds to a concentration of both positive and negative ions of 1.7×10^{-7} mol/m^3. It is clear that the ion concentration in neutral (uncharged) ethanol is two orders of magnitude higher than the difference in concentration of both ions needed to obtain the necessary bulk charge density. This seems likely to support the hypothesis presented. Moreover, the increase of leakage current (see Fig. 4) at higher voltages can be caused by an additional transport of charges (ions). The presence of the EHD flow in the bubble formation, as proposed by Ogata (10), does not seem likely here because this phenomenon occurs at higher voltages only and, besides, the EHD force acting upward could not lower the polarization forces predicted by our model.

CONCLUSIONS

The experimental results indicate two separate regimes of bubble formation, depending upon the applied electric field and particularly on the existence of corona discharges. The formation of bubbles in the absence of corona discharges agrees with a modified form of the Mersmann model by adding an electric force term to the balance of forces acting on the bubble at the moment of detachment. The model predicts the experimentally observed reduction in bubble sizes with the applied voltage assuming the electric force is due to polarization effects. The present model is flexible enough to incorporate effects due to bulk charges which can be present in a liquid at higher electric fields resulting in reduction of polarization forces.

NOTATION

d	capillary inner diameter (m)
d_B	bubble diameter (m)
E	electric field strength (V/m)
F_b	force on bubble due to buoyancy (N)
F_d	force on bubble due to drag (N)
F_e	force on bubble due to electric effects (N)
F_s	force on bubble due to surface effects (N)
g	acceleration due to gravity (m/s^2)
K	constant in Eq. (3) (dimensionless)
P_e	electric stress (N/m^2)
Q	flow rate of gas (m^3/s)
V	applied dc voltage (V)
ρ	density (kg/m^3)

ε permittivity (F/m)
σ interfacial tension (N/m)

Subscripts

n normal
t tangential
x coordinate measured along the perimeter line from the contact point between the bubble and the capillary tip
1 liquid phase
2 gas phase

REFERENCES

1. K. J. Ptasinski and P. J. A. M. Kerkhof, "Electric Field Driven Separations: Phenomena and Applications," *Sep. Sci. Technol.*, *27*, 995 (1992).
2. H. S. Muralidhara, "Enhance Separations with Electricity," *Chemtech.*, *24*, 36 (1991).
3. L. C. Waterman, "Electrical Coalescers," *Chem. Eng. Prog.*, *61*(10), 51 (1965).
4. J. M. Bollinger and R. A. Adams, "Electrofiltration of Ultrafine Aqueous Dispersions," *Ibid.*, *80*(11), 54 (1984).
5. T. C. Scott, "Use of Electric Fields in Solvent Extraction: A Review and Prospectus," *Sep. Purif. Methods*, *18*, 65 (1989).
6. J. C. Giddings, M. N. Myers, and K. D. Caldwell, "Field-Flow Fractionation: Methodological and Historical Perspectives," *Sep. Sci. Technol.*, *16*, 549 (1981).
7. A. A. Zaky and A. Nosseir, "Bubble Injection and Electrically Induced Hydrostatic Pressure in Insulating Liquids Subjected to Nonuniform Fields," *J. Phys. D*, *10*, L189 (1977).
8. M. Sato, Y. Takano, M. Kuroda, and T. Sakai, "A New Cloudy-Bubble Tracer Generated under Electrostatic Field," *J. Chem. Eng. Jpn.*, *13*, 326 (1980).
9. S. Ogata, K. Shigehara, T. Yoshida, and H. Shinohara, "Small Bubble Formation by Using Strong Nonuniform Electric Field," *IEEE Trans. IAS*, *16*, 766 (1980).
10. S. Ogata, K. Tan, K. Nishijima, and J. S. Chang, "Development of Improved Bubble Disruption and Dispersion Technique by an Applied Electric Field Method," *AIChE J.*, *31*, 62 (1985).
11. E. J. M. van Heesch, R. H. P. Lemmens, B. Franken, K. J. Ptasinski, and F. L. S. Geurts, "Pulsed Corona for Breaking Up Air Bubbles in Water," *IEEE Trans. DEI*, *1*, 426 (1994).
12. P. T. Shea and S. M. Barnett, "Flotation Separation Using Microgas Dispersions," *Sep. Sci. Technol.*, *14*, 757 (1979).
13. M. Sato, M. Kuroda, and T. Sakai, "Effect of Electrostatics on Bubble Formation," *Kagaku Kogaku Ronbunshu*, *5*, 380 (1979).
14. C. G. Garton and Z. Krasucki, "Bubbles in Insulating Liquids: Stability in an Electric Field," *Proc. R. Soc. London, A280*, 211 (1964).
15. A. Mersmann, "Druckverlust und Schaumhöhen von Gasdurchströmten Flüssigkeitsschichten auf Siebböden," *VDI-Forschungsh.*, *491, Ausgabe B, Band 28* (1962).
16. H. Tsuge, "Hydrodynamics of Bubble Formation from Submerged Orifices," in *Encyclopedia of Fluid Mechanics, Vol. 3: Gas–Liquid Flows* (N. P. Cheremisinoff, Ed.), Gulf Publishing Co., Houston, 1986, p. 191.

17. K. C. Kao, "Some Electromechanical Effects on Dielectrics," *Br. J. Appl. Phys.*, *12*, 620 (1961).

18. Ansoft Corporation, Pittsburgh, Pennsylvania, *Maxwell 2D Field Simulator*, Finite Element Software Package for a 386 pc.

19. G. Verkerk, J. B. Broens, and W. Kranendonk, *BINAS informatieboek*, Wolters-Noord-hoff, Groningen, 1986 (in Dutch).

Received by editor September 18, 1994